25th ABCM International Congress of Mechanical Engineering
October 20-25, 2019, Uberlândia, MG, Brazil

COB-2019-1762
COMPARATIVE ANALYSIS OF TWO AIRFOILS FOR POSSIBLE UTILIZATION IN SMALL WIND TURBINES

Pedro Antonio Assad Baracat
Faculdade de Engenharia Mecânica da Universidade Estadual de Campinas - FEM/UNICAMP. Rua Mendeleyev 200, Cidade Universitária "Zeferino Vaz", Barão Geraldo, 13083-860, Campinas – SP
Instituto de Pesquisas Eldorado. Av. Alan Turing 275, Cidade Universitária, Barão Geraldo, 13083-898, Campinas – SP
pedroaab@gmail.com

Célia Vanda Alves de Godoy Rosolen
Raquel Miguez de Carvalho
Kamal Abdel Radi Ismail
Willian Minoru Okita
Tomaz Nascimento Morais
Faculdade de Engenharia Mecânica da Universidade Estadual de Campinas - FEM/UNICAMP. Rua Mendeleyev 200, Cidade Universitária "Zeferino Vaz", Barão Geraldo, 13083-860, Campinas – SP
c.rosolen@uol.com.br, raquel.miguezcarvalho@gmail.com, kamal@fem.unicamp.br, minoruokita@gmail.com, tomaznmorais@gmail.com

Francisco Olimpio Moura Carneiro
Faculdade de Engenharia Mecânica da Universidade Estadual de Campinas - FEM/UNICAMP. Rua Mendeleyev 200, Cidade Universitária "Zeferino Vaz", Barão Geraldo, 13083-860, Campinas – SP
Universidade da Integração Internacional da Lusofonia Afro-Brasileira. Avenida da Abolição, 3, Centro, 62790-000, Redenção - CE
olimpiomcarneiro@gmail.com

Abstract. *The Brazilian national energy matrix is composed principally by hydraulic energy. Extending the distribution grid to areas of low population density, long distances from the main grid, remote areas of difficult access and isolated areas usually is not viable and must be attended by alternative ways. Small installation of alternative energy resources such as wind, solar and residual biomass incinerators are among the strong candidates for these sites. The objective of this study is to compare the efficiency of two different airfoils, the S809 airfoil, commonly used for this purpose, and the NACA 4412 airfoil, used in aircraft propulsion, for a nominal power generation of 10 kW with an average wind speed of 8.73 m/s, which is found in some regions in Northeast of Brazil. This work reports the influence of the geometry and operating conditions on the power coefficient. The blade element method (BEM) is implemented in a Matlab home built code which was optimized and validated against available experimental results. The pitch and chord distributions along the blade, the axial and tangential induction factors, the distribution of thrust, torque and power and the annual generated power were calculated and commented.*

Keywords: *wind energy, NACA 4412, S809, Blade Element Momentum, small wind turbine*

1. INTRODUCTION

Brazil is the 5th largest country in the world. Consequently, it has severe electric power distribution challenges. Its distribution system is almost all connected through the *Sistema Interligado Nacional* (SIN) with current electric losses of about 15 %, mainly due to transmission and distribution due to the large distance between power plants and consumption centers (INPE, 2017). The use of wind generators is an excellent alternative to complement the energy matrix and reduce the use of diesel generators, as they are quieter and less polluting, and use a clean, renewable, free energy source (Alvarez *et al.*, 2008). However, the large-scale integration of wind energy sources also has economic, environmental, social and technical impacts that need to be investigated and minimized (Shafiullah *et al.*, 2013).

Wind power generation varies with wind turbine configurations and operating conditions. Fischer *et al.* (2014) calculated the effect of changes in blade and airfoil geometry on turbine performance for Horizontal-Axis Wind Turbine (HAWT) with a rotor diameter of 82 m and a rated power of 1.5 MW. Using the Computational Blade Optimization and Load Deflation Tool, they concluded that the reduction in the curvature of the airfoils leads to an improved *L/D* ratio in the design range and the reduction in the blade chord resulted in a lower blade thrust. The instability of the operating conditions was evaluated by Karbasian *et al.* (2016), the effect of the S809 airfoil moving with different accelerations in

normal direction to free steam in the boundary layer detachment in the blade profile was calculated using the finite volume method, the SIMPLE algorithm and the shear stress transport model. They concluded that the higher acceleration caused the airfoil to have a positive lift even at negative angles of attack and that when the operating condition was changed from unstable to stable, the aerodynamic characteristics were changed even if the angle of attack was maintained constant.

To design wind turbines, many factors must be considered before selecting a final configuration. The environment where it will be installed is the most important. (Thresher and Dodge, 1998). After designing the turbine according to the environment, some modifications can be made to improve its efficiency. In the literature it is possible to find several proposals of improvements in the wind turbines and also indicating the current interest in this type of technology as a sustainable and environment friendly alternative source of energy (Carrasco *et al.*, 2016; Kazemi *et al.*, 2016; Wang *et al.*, 2017).

This study aims to compare the total power generated by two different types of HAWT, based on two airfoil sections, that is NACA 4412 and S809. The BEM method was used in the analysis. Simulations based on Matlab code were conducted for three fixed Tip Speed Ratio (*TSR*), a linear chord and three pitch curves (two linear and one non-linear). The wind data from São Miguel do Gostoso-RN and a nominal power of 10 kW were adopted for the simulations.

2. METHODOLOGY

Two aerodynamic profiles were selected for the rotor design S809 and NACA 4412 (Fig. 1). The S809 is designed for HAWT applications. This profile maintains the value of the drag coefficient, C_d, with little change in relation to the lift coefficient, C_l. Therefore, for different angles of attack, the value of C_d suffers little variation. The NACA 4412 profile is used for low-speed aviation. Although its characteristics may not be compatible with the requirements for wind turbine application, it is a consolidated and widely tested profile (Alvarez *et al.*, 2008).

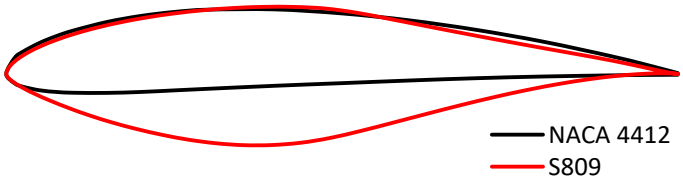

Figure 1. Comparison between NACA 4412 and S809 aerodynamic profiles

2.1 Blade Element Momentum Theory

The basic principle of BEM is to assume that the rate of change of the momentum in the disk is equal to the change in the momentum of the flow within the current tube and that the flow inside the stream tube or expansion cone is not influenced by the external flow (Burton *et al.*, 2001).

The axial and tangential velocities for the calculation of the momentum are reduced by the axial induction factor, a, and the radial induction factor, a'.

The dimension of the blade geometry is applied to a ring of thickness, δr, along the rotor.

The rotor radius can be calculated by (Canale *et al.*, 2018):

$$R = \sqrt{\frac{2P}{\rho \pi U_{\infty}^{3} Cp_{max} \eta_m}} \tag{1}$$

where η_m is the efficiency of the rotor and Cp_{max} is the maximum coefficient of power which considers the Betz limit, wake rotation, blade drag and tip losses due to finite number of blades and is calculated as (Jansen and Smulders, 1977):

$$Cp_{max} = \left(1 - \frac{1.386}{N} sin\frac{\phi}{2}\right)^2 \frac{16}{27}\left(exp\left(-0.35\lambda^{-1.29}\right) - \frac{C_d}{C_l}\lambda\right) \tag{2}$$

where ϕ is function of λ and its values are shown in Jansen and Smulders (1977).

The calculation of the chord in each section of the blade is given for a = 1/3 by:

$$c = \frac{8\pi R \lambda \mu^2 a'}{N C_l \sqrt{(1-a)^2 + \left(\lambda\mu(1+a')\right)^2}} \tag{3}$$

where, R is the rotor radius, λ is *TSR*, μ is the dimensionless radial position (r/R), N is the number of blades and C_l is the lift coefficient of the profile in the condition of maximum lift/drag ratio.

The value of *TSR* for the blade dimensioning is fixed as a boundary condition for the calculation. The *TSR* is given by:

$$\lambda = TSR = \frac{\Omega R}{U_\infty} \tag{4}$$

where Ω is the angular velocity of the rotor and U_∞ is the free stream velocity.

The values of a and a' are related, observing that a' varies radially along the blade, as in:

$$a' = \frac{a(1-a)}{\lambda \mu^2} \tag{5}$$

The local inflow angle, ϕ, the local angle of attack, α, and the local angle of pitch, θ, required to maintain α in the ideal lift/drag condition are shown in Fig. 2.

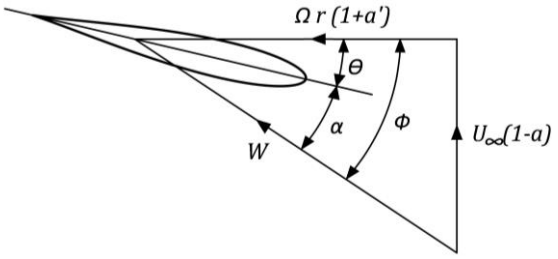

Figure 2. Composition of the flow angles in each section. Adapted from Burton *et al*. (2001)

2.2 Numerical analysis

In this work, BEM theory with Prandtl and Glauert corrections were applied in a low computational effort Matlab algorithm. The nominal conditions for this study are: power equal 10 kW, average wind speed equal 8.73 m/s, density of the air equal 1.225 kg/m^3, dynamic viscosity of the air equal 1.83x10^{-5} Pa.s, mechanical efficiency of 0.9 (Canale *et al*., 2018), 3 blades and NACA 4412 and S809 airfoil profiles.

The first iterative process starts with the value of the wind speed. The rotational speed of the turbine is calculated using Eq. (4). In the sequence, the second iterative process defined by the blade elements starts from the blade hub to the blade tip. For each blade element the local angle of pitch, θ, the chord, c, and the solidity, σ, are obtained. The third iterative process begins with the initial guess of axial induction factor, a, and tangential induction factor, a', proceeding to the calculation of new values. The local flow velocity, W, the local inflow angle, ϕ, the local Reynolds number and Mach number values are calculated. The values of C_l and C_d with α were calculated from JavaFoil (Hepperle, 2018) and incorporated as file in the Matlab code for different values of Reynolds number. For each iteration process, a search for the closest Reynolds number is used.

The Prandt's tip loss factor considers the effects of the finite number of blades. In this work the effects of the hub are considered in a similar way. Thus, the total loss factor, F, is calculated by:

$$F = \left(\frac{2}{\pi}\cos^{-1}\left(\exp\left(-\frac{N(R-r)}{2r\sin\phi}\right)\right)\right)\left(\frac{2}{\pi}\cos^{-1}\left(\exp\left(-\frac{N(r-R_{hub})}{2r\sin\phi}\right)\right)\right) \tag{6}$$

From the conservation of momentum of the flow and the aerodynamic force component in the axial and tangential direction to the plane of the rotor, the new values a and a' are obtained with the following equations adapted from Hansen (2008) with Glauert and Spera correction for high values of a:

$$a = \begin{cases} (K+1)^{-1} & , \; a \le a_c \\ \frac{1}{2}\left(2 + K(1-2a_c) - \sqrt{\left(K(1-2a_c)+2\right)^2 + 4\left(Ka_c^2 - 1\right)}\right) & , \; a > a_c \end{cases} \tag{7}$$

$$a' = \left(\frac{4F \sin\phi \cos\phi}{\sigma\left(C_l \sin\phi - C_d \cos\phi\right)} - 1 \right)^{-1} \tag{8}$$

where $a_c = 0.2$ (Hansen, 2008) and the variable K is given by:

$$K = \frac{4F \sin^2\phi}{\sigma\left(C_l \cos\phi + C_d \sin\phi\right)} \tag{9}$$

The gradient of thrust, *dT/dr*, and torque, *dQ/dr*, are calculated by:

$$\frac{dT}{dr} = \frac{1}{2} F \rho W^2 Nc \left(C_l \cos\phi + C_d \sin\phi\right) \tag{10}$$

$$\frac{dQ}{dr} = \frac{1}{2} F \rho W^2 Ncr \left(C_l \sin\phi - C_d \cos\phi\right) \tag{11}$$

The thrust and torque are calculated by the sum of the contribution from each blade element.
The generated power, *P*, can be calculated by multiplication of the torque by the angular velocity of the rotor, as:

$$P = Q\Omega \tag{12}$$

The maximum available power within the disc is given by:

$$P_{max} = \frac{1}{2} \rho \pi R^2 U_\infty^3 \tag{13}$$

The power coefficient, C_p, is calculated from:

$$C_p = \frac{P}{P_{\mathbf{max}}} \tag{14}$$

2.3 Annual energy production

The Weibull distribution was used to give a good representation of the probability of the hourly variation in the wind speed over a year. The probability density function is given by (Burton *et al*., 2001):

$$f\left(V\right) = k \frac{U_\infty^{k-1}}{c^k} exp\left(-\left(\frac{U_\infty}{c} \right)^k \right) \tag{15}$$

The probability for the wind speed was calculated for São Miguel do Gostoso-RN (5.13° W, 35.64° S). The average speed is 8.73 m/s, factor *c* is 9.81 and factor *k* is 2.79 from 50 m above the ground (Cresesb, 2019).

3. GRID TEST AND VALIDATION

The number of elements simulated in the grid test were 5, 10, 30, 50 and 400 elements for NACA 4412, *TSR* equal 5. The results for power for each grid and the percentage difference between the grid and the previous grid are shown in Tab. 1.

Table 1. Grid test

Number of elements	5	10	30	50	400
Power (W)	8536	8049	7960	7904	7895
Percent difference (%)		5.705	1.106	0.704	0.114

The number of elements chosen for this work was 50, because the corresponding result is close enough to 0.114 % while the computational time is significantly reduced.

To verify the accuracy of the numerical simulation, a comparison with experimental data presented by Hansen (2008) for the turbine Nordtank NTK using 50 blade elements was made and the results were presented in Fig. 3. The airfoil is FF-W3-211 (Bak *et al*., 1999) with 3 blades, a 20.5 m of rotor radius, 22 % of hub, non-linear chord and twist and a constant angular speed equal 27.1 rpm.

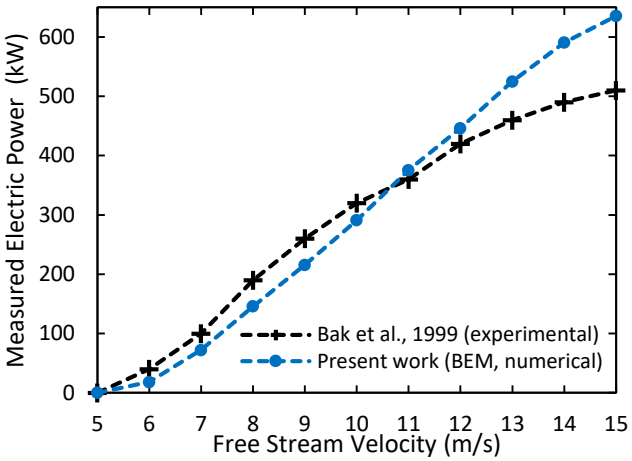

Figure 3. Comparison of the predicted power variation with the available measured data

Figure 3 shows that the present results are close to the available results up to wind speed of 13 m/s, specifically for this case. The calculated curve follows the trend of the experimental curve. The maximum deviation between the values calculated by the present method and the experimental values is -23 % at a speed of 8 m/s and +14 % at a speed of 13 m/s. For wind speeds above 13 m/s, the simulation began to diverge due the Glauert and Spera correction behaves better for small wind speeds and cannot predict losses associated with high speeds.

4. RESULTS AND DISCUSSION

4.1 Implementation of the BEM Theory

The implementation of the equations from subsection 2.1 was done for both airfoils for an axial induction factors equal 1/3 and *TSR* equal 4, 5 and 6 in a spreadsheet and the discretization of the blade was performed. The average speed is 8.73 m/s from São Miguel do Gostoso-RN from 50 m above the ground (Cresesb, 2019). The radius to achieve the 10 kW of nominal power for this wind speed is 4.16 m for *TSR* equal 4, radius of 4.12 m for *TSR* equal 5 and radius of 4.10 m for *TSR* equal to 6 for NACA 4412 profile. For S809 profile the radius to achieve the same nominal power is 4.18 m for *TSR* equal 4, radius of 4.14 m for *TSR* equal 5 and radius of 4.12 m for *TSR* equal 6. The hub is adopted 10 % of the rotor radius. Figure 4 shows the results for the turbine based on airfoil NACA 4412 and *TSR* equal 6 and Fig. 5 shows the results for the airfoil S809 and *TSR* equal 5.

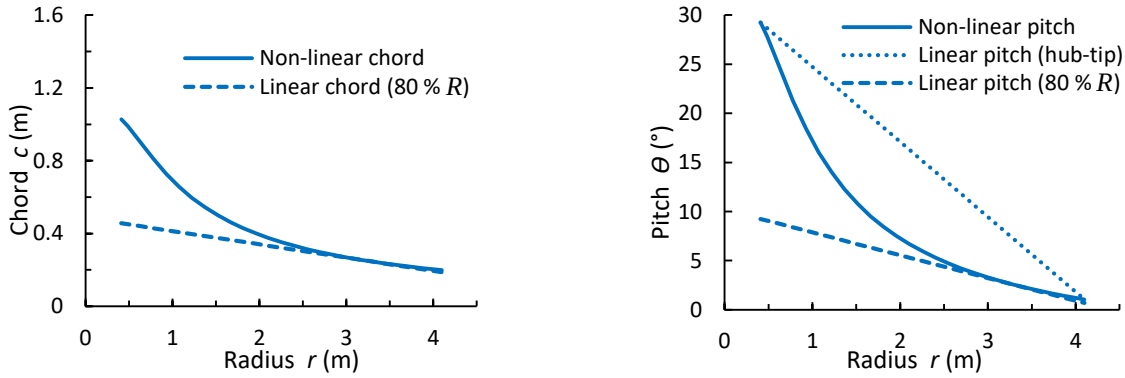

a) Chord curve b) Pitch curve

Figure 4. Blade geometry for NACA 4412 for *TSR* equal 6

The blade geometry for the non-linear chord is complex to manufacture and linearization of the chord can simplify its construction (Burton *et al.*, 2001). This simplification is done by drawing a line tangent to the non-linear chord distribution at the point *r* equal 80 % *R* (reference point) (Fig. 4a and 5a). Three different curves of pitch distribution along the blade were investigated, ie, non-linear distribution, linear distribution from hub to tip and linear pitch distribution tangent to the refence point (Fig. 4b and 5b).

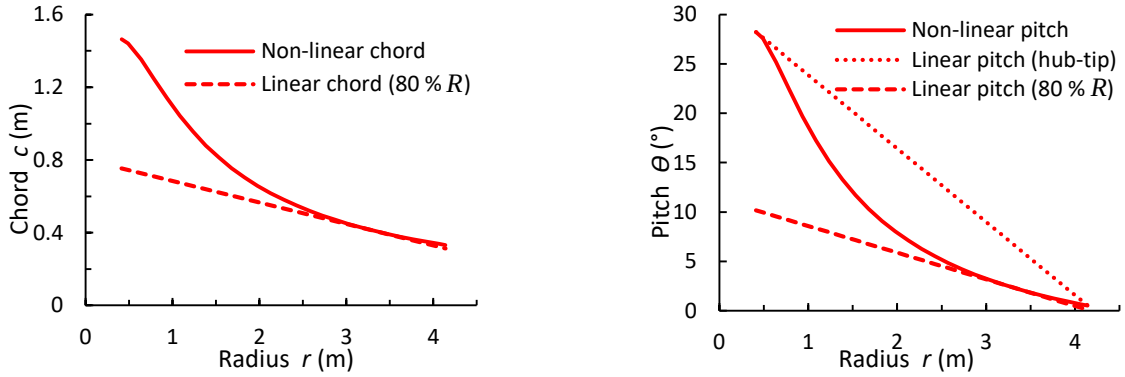

a) Chord curve b) Pitch curve

Figure 5. Blade geometry for S809 for *TSR* equal 5

The NACA 4412 profile presents the best C_l/C_d ratio for angle of attack equal to 5.25°, with C_l = 1.052 and C_d = 0.0081 (Re=1.0x10^6). And the S809 profile presents the best C_l/C_d ratio for angle of attack equal to 7° with C_l = 0.911 and C_d = 0.0084 (Re=1.0x10^6).

4.2 Analysis of numerical results

The home-built code was applied for 50 elements using BEM theory with Prandtl, Glauert and Spera corrections and iterative calculation of the axial and the tangential induction factors. The simulations were performed for a *TSR* equal 4, 5 and 6, with a rotor radius of 4.16 m, 4.12 m and 4.10 m, respectively, for NACA 4412 and with a rotor radius of 4.18 m, 4.14 m and 4.12 m respectively for S809, with 10 % of hub, a reference wind speed of 8.73 m/s and three variations of the pitch angle along the blade as shown in Fig. 4b and 5b. Table 2 shows the results of power, power coefficient, thrust and torque for all simulated cases.

Table 2. Power and Power coefficient for each simulated case for the average wind speed

Airfoil	*TSR*	Pitch distribution	Power (W)	Power coefficient	Thrust (N)	Torque (Nm)
NACA4412	4	Non-linear	7553	0.3409	1594	899.8
NACA4412	4	Linear (hub-tip)	6938	0.3131	1234	826.5
NACA4412	4	Linear (80 % *R*)	7192	0.3246	1658	856.8
NACA4412	5	Non-linear	7904	0.3637	1626	746.0
NACA4412	5	Linear (hub-tip)	6647	0.3059	1092	627.4
NACA4412	5	Linear (80 % *R*)	7526	0.3463	1667	710.4
NACA4412	6	Non-linear	8203	0.3811	1658	642.0
NACA4412	6	Linear (hub-tip)	5984	0.2781	977.3	468.4
NACA4412	6	Linear (80 % *R*)	7862	0.3653	1711	615.4
S809	4	Non-linear	7651	0.3420	1668	915.8
S809	4	Linear (hub-tip)	7273	0.3251	1288	870.6
S809	4	Linear (80 % *R*)	6780	0.3031	1649	811.6
S809	5	Non-linear	7824	0.3566	1736	742.1
S809	5	Linear (hub-tip)	6947	0.3166	1129	658.9
S809	5	Linear (80 % *R*)	6924	0.3155	1724	656.7
S809	6	Non-linear	7812	0.3595	1716	614.5
S809	6	Linear (hub-tip)	6251	0.2877	999.3	491.7
S809	6	Linear (80 % *R*)	6950	0.3198	1700	546.7

Table 2 shows that the highest performance for NACA 4412 and S809 are for non-linear pitch angle for all *TSR*, due to distribution of angle of attack along the blade near to that for $C_l/C_{d\,max}$. The airfoil NACA 4412 produces higher generated power than S809, due to the high values of C_l/C_d.

Furthermore, at each *TSR* value (Tab. 2), it is possible to notice that the highest thrust values are associated to the linear pitch (80 % *R*), and the lowest thrust values are associated to the linear pitch (hub-tip) case, for the NACA 4412 airfoil profile. Between them are the thrust values for the non-linear pitch case. For the S809 airfoil profile, the lowest thrust values are also associated to the linear pitch (hub-tip). The middle thrust values for the S809 are associated to the linear pitch (80 % *R*), and highest thrust values are associated to the non-linear pitch case, in an opposite way of NACA 4412. However, for both airfoils, the values of thrust for the linear pitch (80 % *R*) and non-linear pitch cases are close and significantly higher than the thrust values for the linear pitch (hub-tip) case.

Regarding the torque values presented in Table 2 (at each *TSR*), the highest values are found for the non-linear pitch case, for both NACA 4412 and S809 airfoil profiles. The lowest values of torque for the NACA 4412 at all *TSR* cases, and for the S809 at a *TSR* of 6 are found for the linear pitch (hub-tip) distribution, which may lead to lower power and power coefficients. Medium values of torque for the NACA 4412 are found for linear pitch (80 % *R*). For the S809, medium values of torque are found for the linear pitch (hub-tip), at *TSR* values of 4 and 5. Analyzing the thrust and torque values from a global perspective, the non-linear pitch distribution seems to present the best potential in terms of performance.

Therefore, *TSR* equal 6 achieved the highest generated power and power coefficient for NACA 4412, yet for S809, *TSR* equal 5 achieved the highest generated power. Therefore, the turbine with the NACA 4412 airfoil profile, with a fixed *TSR* of 6, with a linear chord and non-linear pitch and the turbine with S809 airfoil profile, with a fixed *TSR* of 5, with a linear chord and non-linear pitch were chosen for comparison. The thrust and torque distributions, the axial and tangential induction factors along the blade are shown in Fig. 6 and 7 and the generated power and power coefficient with free stream velocity are shown in Fig. 8 for both chosen cases.

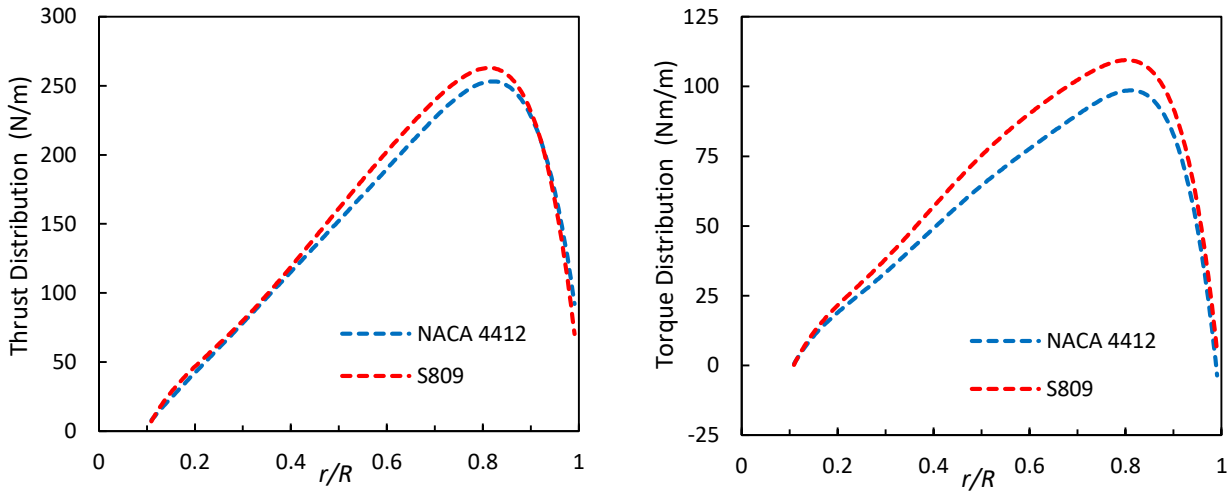

a) Thrust distribution b) Torque distribution

Figure 6. Blade load distribution along the blade for both airfoils

Both rotors with NACA 4412 and S809 airfoil profiles present similar distributions of thrust and torque along the blade (Fig. 6), which are higher for the S809. The axial induction factor curves are also similar for both airfoils (Fig. 7b), with higher values for the S809. While the tangential induction factor curve presents higher values for the S809, with a regular distance between them along the radius (Fig. 7a), the axial induction factor curves show more pronounced differences around $r/R = 0.7$ and the lowest differences close to the root and tip. The torque curve shows the same behavior, with a higher difference around $r/R = 0.7$ and the lowest differences close to the hub and tip. Therefore, the results show a coherent relation between torque and axial induction factor and between thrust and tangential induction factor.

The thrust and torque distribution along the blade for rotors based on NACA 4412 and S809 airfoil profiles are similar (Fig. 6), with higher for the S809. The lift and drag forces are directly influenced by the chord, camber and local wind velocity. The local relative velocity depends on the angular velocity of the rotor (or *TSR*) as well as on the induction factors. In turn the lift and drag coefficients of NACA 4412 and S809 may present high differences due to their shapes and to the angle of attack.

The rotors with NACA 4412 and S809 airfoils present similar curves and values for the generated power (Fig. 8a), with higher values for the NACA 4412. The power coefficient curves are also similar (Fig. 8b) and shows good behavior in relation to the expected constant form at the operation with fixed *TSR* (Burton *et al.*, 2001). From Table 2, the

NACA 4412 rotor shoows a thrust of 1658 N and a torque of 642 Nm for a *TSR* of 6, while for the S809 the values are 1737 N and 742.1 Nm, respectively, at a *TSR* of 5, for wind velocity of 8.73 m/s. Each of the torque values multiplied by the angular velocity of the respective rotor, Eq. (12), provides the power generated by the turbine, whose values are in Fig. 8a.

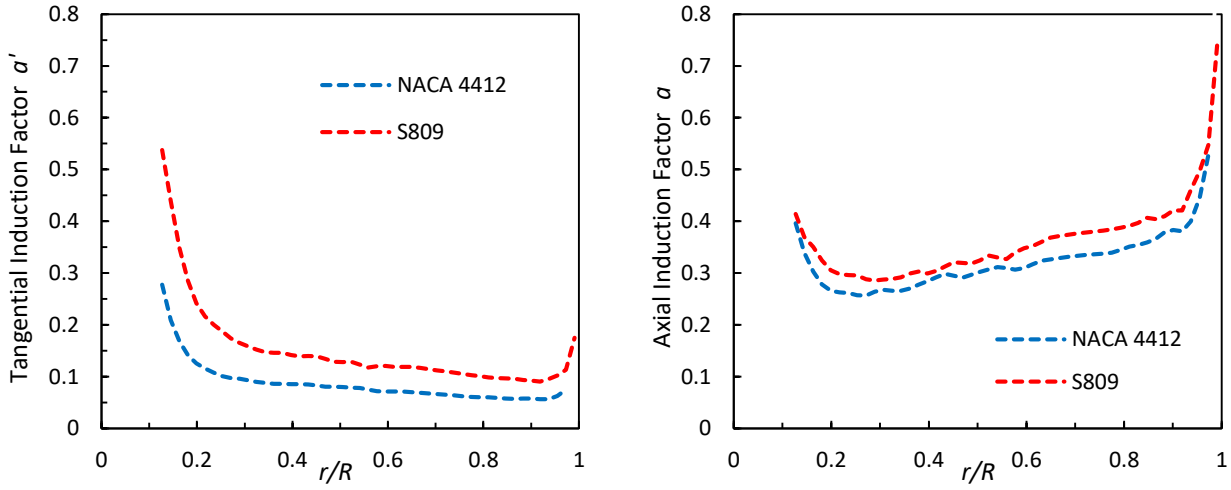

a) Tangential induction factor b) Axial induction factor

Figure 7. Induction factors along the blade for both airfoils

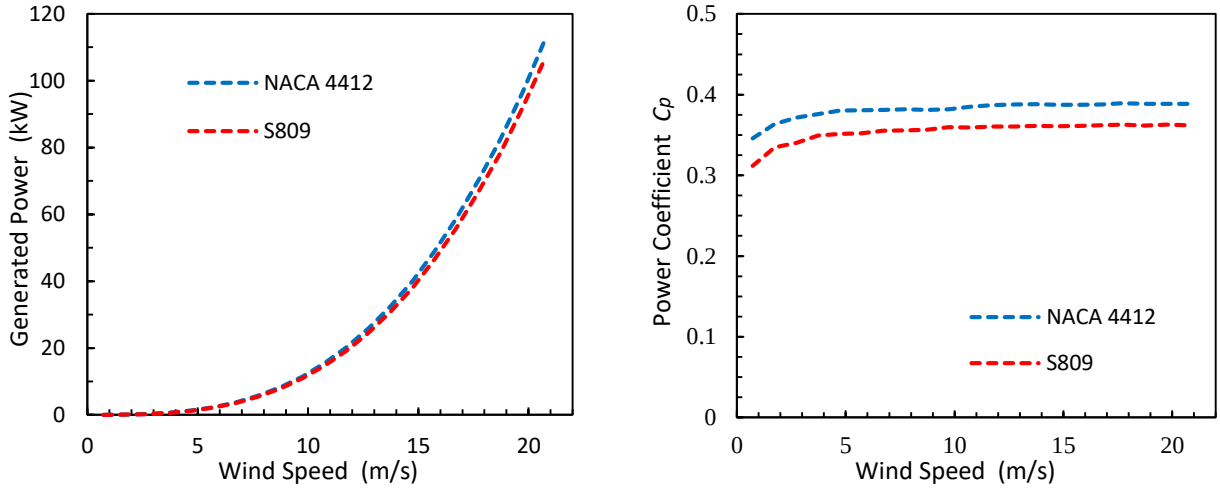

a) Generated power b) Power coefficient

Figure 8. Power and power coefficient with free stream velocity

4.3 Annual energy production

Finally, the annual energy production was evaluated based on the probability of the Weibull distribution for wind speed and the generated power for the chosen case for NACA 4412 and S809 (Fig. 9).

The annual energy production curve is shifted relative to the probability curve because the generated power at higher wind speeds is greater than at lower wind speeds (Fig. 8a), compensating the lower values for the probability of velocities greater than the average wind speed. The peak of annual energy production occurs at a wind speed of around 11.73 m/s for both wind turbines, with NACA 4412 and S809 airfoil profiles. Then, as the velocity increases, the probability decreases a lot and the annual energy output falls as well.

The annual energy production for the wind turbines with NACA 4412 and S809 profiles are 106704.9 kWh and 101479.1 kWh, respectively. If we take as a reference the value given by Hansen (2008), which is 1.090 GWh of annual production corresponds to the consumption of 250 houses, approximately, the annual output of the wind turbine with NACA 4412 profile would provide energy for consumption of 24 houses, while the S809 profile turbine would provide energy for about 23 houses.

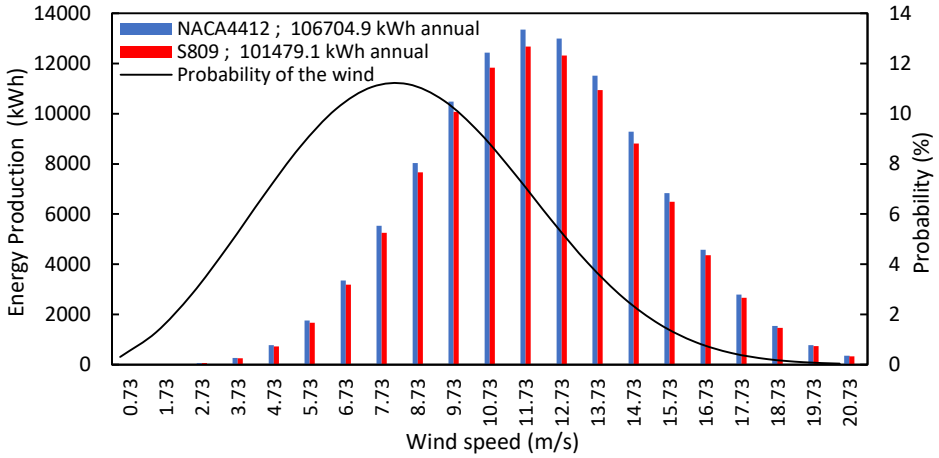

Figure 9. Energy production of the wind turbines with NACA 4412 and S809 and probability of the Weibull distribution for wind speed in São Miguel do Gostoso-RN

5. CONCLUSION

In this study the authors present a numerical investigation on a small horizontal axis wind turbine with 3 blades and with a fixed tip speed ratio. A home-built code based on the BEM theory was developed and validated against experimental available results. A comparison of the total power generated by two different airfoil profiles were made using the wind speed data from São Miguel do Gostoso-RN. The principal results obtained in this study were:

- The non-linear pitch curve achieved higher generated power and power coefficient than both linear pitch curves for all simulated *TSR*.
- *TSR* equal 6 was chose for NACA 4412 and *TSR* equal 5 was chose for S809 due to the highest generated power.
- The NACA 4412 based-rotor is found to produce an annual energy production of 106704.9 kWh, while the S809 based-rotor produced an annual energy production of 101479.1 kWh or a difference of 4.9 %. The generated energy is sufficient for 24 homes.

6. ACKNOWLEDGEMENTS

The authors wish to thank the *Instituto de Pesquisas Eldorado* (Eldorado Research Institute) for the financial support for the first author, the *Coordenação de Aperfeiçoamento de Pessoal de Nível Superior* (CAPES) for the financial support for the third and fifth authors, and the *Conselho Nacional de Desenvolvimento Científico e Tecnológico* (CNPq) for the PQ Research Grant to the fourth author.

7. REFERENCES

Alvarez, A.C.C., Rocha, P.A.C. and Carneiro, F.O.M., 2008. “Projeto aerodinâmico de um gerador eólico tripá para ventos de baixa intensidade, utilizando a teoria do momento do elemento de pá”. In *Proceedings of the V Congresso Nacional de Engenharia Mecânica - CONEM-2008*, Salvador, Bahia, Brazil - CON08-1776.

Bak, C., Fuglsang, P., Sorensen, N.N., Aagaard Madsen, H., Shen, W. Z., Sorensen, J. N., 1999. “Airfoil characteristics for wind turbines”. Denmark. Forskningscenter Risoe. Risoe-R, No. 1065(EN)

Burton, T., Sharpe, D. and Jenkins, N., 2001. *Handbook of wind energy*. John Wiley & Sons.

Canale, T., Ismail, K. A. R., Lino, F.A.M., 2018. “Aerodynamic evaluation of Gottingen and Joukowski airfoils for use in rotors of small wind turbines. In *Proceedings of the 10th International Conference on Rotor Dynamics – IFToM 2018.* Mechanisms and Machine Science, Vol. 63, pp. 531-543. Springer, Cham

Carrasco, A.D.V., Valles-Rosales, D.J., Mendez, L.C. and Rodriguez, M.I., 2016. “A site-specific design of a fixed-pitch fixed-speed wind turbine blade for energy optimization using surrogate models”. *Renewable Energy*, Vol. 88, pp. 112 – 119. ISSN 0960-1481. doi: https://doi.org/10.1016/j.renene.2015.11.018.

Cresesb, 2019. “Centro de Referência para Energia Solar e Eólica”. 28 May 2019 < http://www.cresesb.cepel.br/index.phpdata >

Fischer, G.R., Kipouros, T. and Savill, A.M., 2014. "Multi-objective optimisation of horizontal axis wind turbine structure and energy production using aerofoil and blade properties as design variables". *Renewable Energy*, Vol. 62, pp. 506–515.

Hepperle, M., 2018. "JavaFoil – Analysis of Airfoils". 10 May 2019 < http://www.mh-aerotools.de/airfoils/javafoil.htm >

INPE: Instituto Nacional de Pesquisas Espaciais, 2017. "Atlas Brasileiro de Energia Solar". São José dos Campos.

Jansen, W.A.M., Smulders, P.T., 1977. "Rotor design for horizontal axis windmills", vol 7701. SWD publications. Stuurgroep Windenergie Ontwikkelingslanden, Amersfoort.

Karbasian, H.R., Esfahani, J. and Barati, E., 2016. "Effect of acceleration on dynamic stall of airfoil in unsteady operating conditions". *Wind Energy*, Vol. 19, No. 1, pp. 17–33.

Kazemi, S.A., Nili-Ahmadabadi, M., Sedaghat, A. and Saghafian, M., 2016. "Aerodynamic performance of a circulating airfoil section for magnus systems via numerical simulation and flow visualization". *Energy*, Vol. 104, pp. 1–15.

Shafiullah, G., Oo, A.M., Ali, A.S. and Wolfs, P., 2013. "Potential challenges of integrating large-scale wind energy intothe power grid–a review". *Renewable and sustainable energy reviews*, Vol. 20, pp. 306–321.

Thresher, R.W. and Dodge, D.M., 1998. "Trends in the evolution of wind turbine generator configurations and systems". *Wind Energy: An International Journal for Progress and Applications in Wind Power Conversion Technology*, Vol. 1,No. S1, pp. 70–86.

Wang, H., Zhang, B., Qiu, Q. and Xu, X., 2017. "Flow control on the nrel s809 wind turbine airfoil using vortex generators". *Energy*, Vol. 118, pp. 1210–1221.

8. RESPONSIBILITY NOTICE

The authors are the only responsible for the printed material included in this paper.